JOURNAL OF MATERIALS SCIENCE **39** (2004) 5091 – 5096

Fast diffusion in nanocrystalline ceramics prepared by ball milling

PAUL HEITJANS*, SYLVIO INDRIS
Institut für Physikalische Chemie und Elektrochemie, Universität Hannover, Callinstraße 3-3A, 30167 Hannover, Germany
E-mail: heitjans@pci.uni-hannover.de

Nanocrystalline materials can show enhanced diffusivity compared to their microcrystalline counterparts due to the large fraction of atoms or ions located in interfacial regions. In the case of ceramics, resulting properties with potential applications are, e.g., fast ionic conductivity, high mechanical creep rate and increased catalytic activity. Different nanocrystalline ceramic materials were prepared by high-energy ball milling of coarse grained source materials. The samples were characterized by XRD, TEM, BET method and IR spectroscopy. These measurements show that the primary crystallites form larger agglomerates with internal interfaces and that the reduction of the crystallite size is accompanied by a structural degradation of the surface zone. An example is the partial amorphization observed for $LiBO_2$ by IR spectroscopy. The diffusivity and ion conductivity in these materials was studied by NMR relaxation, NMR line shape and impedance spectroscopies. It was possible to discriminate between highly mobile ions in the interfacial regions and immobile ions in the grains. In general diffusion in the nanocrystalline systems was found to be fast compared to that in the corresponding microcrystalline source materials.

1. Introduction

Nanocrystalline powders consist of crystallites with an average size of typically 5 to 50 nm [1, 2]. This entails an enhanced surface area which is an important parameter for applications, e.g., in catalysis. Furthermore, when nanocrystalline powders are compacted they have an increased concentration of grain boundaries which may form fast diffusion pathways for atoms or ions [3, 4]. Fast diffusion of ions is synonymous with a high ionic conductivity which is interesting concerning applications in battery systems, fuel cells or sensors.

A key for understanding the structure-mobility relations in nanocrystalline ceramics is to clarify the microscopic structure of the grain boundaries and also the morphology of the grain boundary network including residual pores and so-called triple junctions. Therefore the present studies of ion diffusion with the two complementary methods of impedance spectroscopy and NMR relaxation techniques have been accompanied by comprehensive structural characterization of the nanocrystalline samples, and the results have been compared with those of the coarse grained and amorphous counterparts.

2. Sample preparation

There are two basic routes to prepare nanocrystalline materials. The first is to assemble the nanocrystals from single atoms or molecules from solution or the gas phase. The other way is to start with coarse grained (microcrystalline) powders and to reduce the average grain size to about one thousandth by mechanical attrition. This has been done in our case by high-energy ball milling [5, 6]. Besides grain size reduction, also phase transformations or, in case that more than one phase is milled, chemical reactions can occur [7–10]. In particular the latter process, however, was not wanted in the present study and precautions were taken to avoid it [5]. We used source materials with an average grain size of some μm, a shaker mill SPEX 8000 and an alumina vial with a single alumina ball. The ball-to-powder weight ratio was typically 2:1. The powders were compacted with an uniaxial pressure of 1 GPa resulting in pellets with a density of about 85% of that in the single crystals.

Following this procedure we prepared nanocrystalline samples of the Li ion conducting oxides $LiBO_2$ and $LiNbO_3$ and the anion conductor BaF_2 as well as of TiO_2, which is interesting for catalytic applications. Furthermore we prepared a composite material of nanocrystalline Li_2O (Li ion conductor) and Al_2O_3 (ion insulator).

The corresponding microcrystalline counterparts taken from the unmilled source materials served as reference samples. In the case of $LiBO_2$ and $LiNbO_3$ also the amorphous counterparts were obtained by

*Author to whom all correspondence should be addressed.

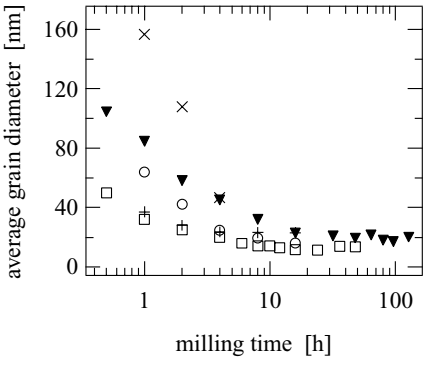

Figure 1 Average grain sizes vs. milling time for some oxide ceramics: $LiBO_2$ (□), $LiNbO_3$ (▼), Li_2O (+), α-Al_2O_3 (○) and TiO_2 rutile (×).

quenching from the melt and by a sol-gel method, respectively [11, 12].

3. Sample characterization

The different nanocrystalline powders were characterized by X-ray diffraction (XRD), transmission electron microscopy (TEM), surface area analysis (BET), differential thermal analysis (DTA) and infrared spectroscopy (IR). With increasing milling time the XRD patterns show an increasing peak broadening which can be used to determine the average crystallite size [13]. Fig. 1 shows results for $LiBO_2$, $LiNbO_3$, Li_2O, α-Al_2O_3 and TiO_2 (rutile) after various milling times. All materials exhibit a similar behaviour with two different time regimes. For milling times of up to about 5 h the average crystallite size decreases with increasing milling time. By this it is possible to adjust the average crystallite size in the range from the μm to the nm regime by choosing of the appropriate milling time. For longer milling times all samples show a saturation behaviour with a final average grain size of about 20 nm.

We performed TEM measurements to check the results for the crystallite sizes. An example is shown in Fig. 2 for TiO_2 (rutile) ballmilled for 4 h. One can see crystallites with sizes of 20 to 30 nm which is in good agreement with the XRD results. The lattice spacing found in this micrograph is 2.3 Å which is equal to $a/2$ in the tetragonal rutile structure.

The BET surface area of the powders was measured using nitrogen adsorption. The results are shown exemplarily for TiO_2 (anatase and rutile) in Fig. 3. For both materials the surface area increases monotonically with increasing milling time and shows again a saturation behaviour which corresponds to that of the crystallite sizes (cf. Fig. 1). The increase in the specific surface area (by a factor of about three in the case of rutile) is much weaker than the decrease in the crystallite sizes (by about three orders of magnitude). This shows that ball milling produces many internal interfaces and not necessarily open surfaces. This is corroborated by the TEM micrographs where agglomerates of nanocrystals are visible.

A phase transformation could be observed during milling of $LiBO_2$. Fig. 4 shows IR spectra of ballmilled $LiBO_2$ in comparison with the unmilled sample and the glassy material [11]. The source material consists of the two crystalline phases α-$LiBO_2$ and γ-$LiBO_2$. The characteristic peaks of different vibration modes of the crystalline phases (e.g. at 634 cm^{-1} for α-$LiBO_2$; 700 cm^{-1} and 775 cm^{-1} for γ-$LiBO_2$) disappear with increasing milling time and the overall spectra of the

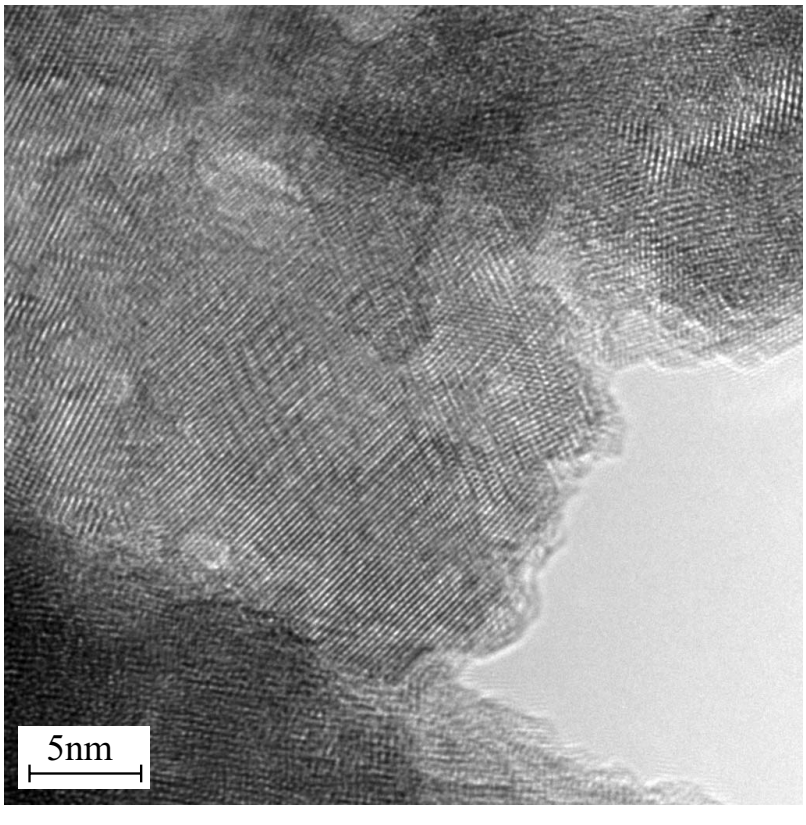

Figure 2 TEM micrograph of TiO_2 (rutile) which has been milled for 4 h resulting in an average grain size of about 40 nm.

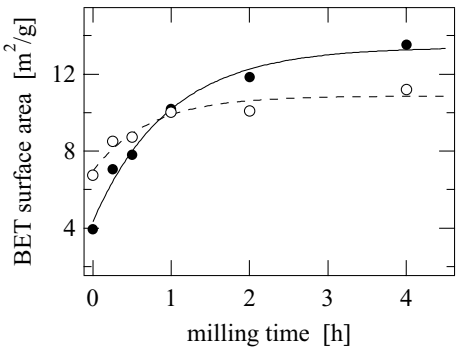

Figure 3 BET surface area of TiO_2 (rutile (●) and anatase (○)) vs. milling time.

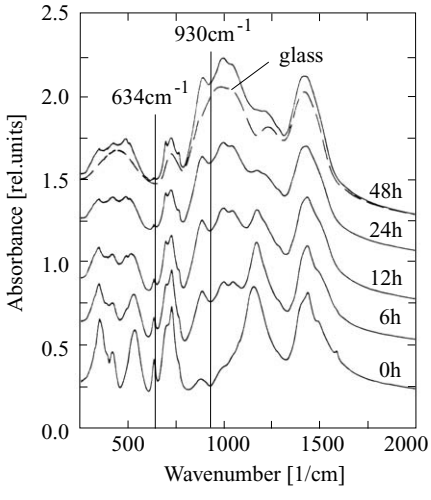

Figure 4 IR spectra of nanocrystalline $LiBO_2$ ballmilled for various times in comparison with glassy $LiBO_2$.

nanocrystalline samples become very similar to that of the glassy material. This shows that, at least in this material being a good glass former, the reduction of the crystallite sizes is accompanied by a phase transformation during milling. The kinetics of the phase transformation is tracked via the dependence of IR intensities at 634 cm^{-1} (crystalline phase) and 930 cm^{-1} (glassy phase) on the milling time. In Fig. 5 these intensities are compared with the intensity of a certain peak in the XRD patterns (at 27.9°2θ for Cu K_α, see [11]) representing the crystalline phase. Furthermore, in Fig. 5 the milling time dependence of the intensity of an exothermic peak found in DTA measurements is shown which has been ascribed to recrystallization of the ballmilled samples and thus represents the amount of the glassy phase produced by the milling process [11]. The vanishing of the crystalline phase seems to be faster than the production of the amorphous phase which may hint at the existence of an interface as transition stage between both phases. However, $LiBO_2$ nanocrystals embedded in the amorphous matrix seem to be present up to the longest milling time.

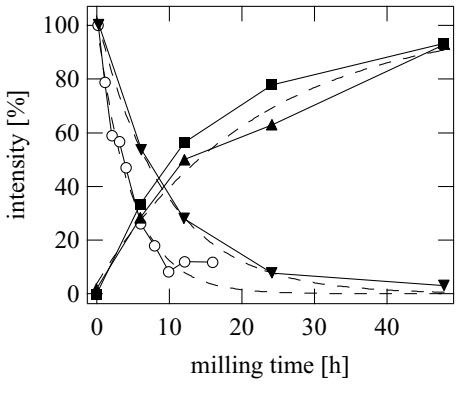

Figure 5 Kinetics of phase transformation in $LiBO_2$ during ball milling: (○) XRD intensity at 27.9° 2θ, (▼) IR intensity at 634 cm^{-1}, (▲) IR intensity at 930 cm^{-1}, (■) fraction of recrystallization according to DTA at 710 K. Data points are interconnected as guide to the eye. Dashed lines are exponential fits.

4. Experimental methods

We used conductivity measurements as well as NMR relaxation techniques to study the long-range and short-range transport, respectively, of ions in the nanocrystalline materials. The dc conductivity σ_{dc} is directly related to the diffusion coefficient D^{dc} and thus to the long-range transport of charge carriers (charge q, number density N) via the Nernst-Einstein relation

$$D^{dc} = \frac{\sigma_{dc} k_B T}{N q^2}. \quad (1)$$

T is the temperature and k_B the Boltzmann constant. When more than one charge carrier is involved discrimination of the different contributions to the overall conductivity has to be done.

Measurements of the NMR spin-lattice relaxation rate T_1^{-1} and NMR lineshape as a function of temperature give access to average residence times τ of specific ions and the activation barriers for single ion jumps [3, 14]. The diffusion coefficient can then be calculated from the Einstein-Smoluchowski relation

$$D = \frac{\ell^2}{6\tau} \quad (2)$$

where ℓ is the average jump length which can be estimated from the lattice parameters of the crystals.

The temperature dependence of the diffusion coefficient can often be described by an Arrhenius relation

$$D = D_0 \exp\left(-\frac{E_A}{k_B T}\right) \quad (3)$$

with a pre-exponential factor D_0 and an activation energy E_A. It has to be noted that the activation energies derived from measurements of the dc conductivity can differ from those derived from NMR measurements. This is due to the fact that in general NMR techniques are probing the short-range motion of the ions and the activation energy represents the barriers for single ion jumps. In contrast to that the dc conductivity describes the long-range motion of the ions where they have to overcome larger barriers on their diffusion pathways.

The NMR measurements on ^7Li and ^{19}F were performed on a solid-state NMR spectrometer (Bruker MSL 100) in combination with a field variable cryomagnet. Temperatures of up to 1000 K were covered with a home-built high-temperature probe. The

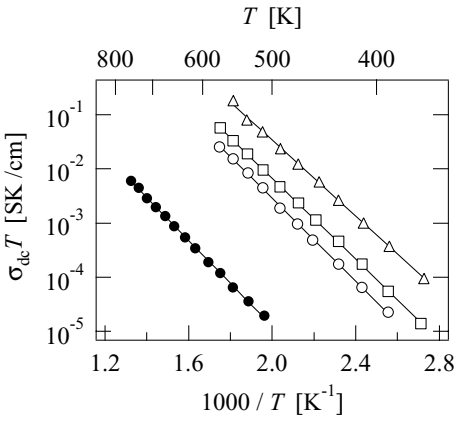

Figure 6 Conductivity of nanocrystalline $LiBO_2$ milled for 12 h (○), 24 h (□), 48 h (△) in comparison with coarse grained (●) $LiBO_2$ [15]. The lines represent fits with an Arrhenius relation.

conductivity measurements were done with a standard impedance analyser (HP 4192A) in the frequency range from 5 Hz to 13 MHz. From these the dc conductivity was extracted by comparison with simple equivalent circuits.

5. Experimental results

In this section we present some case studies of ion diffusion in different nanocrystalline ceramic materials. $LiBO_2$ is a Li ion conductor. The dc conductivity of nanocrystalline $LiBO_2$ prepared by ball milling is shown in Fig. 6 for temperatures between 350 and 600 K together with that of coarse grained $LiBO_2$ [15]. The conductivity of the nanocrystalline $LiBO_2$ increases with increasing milling time and thus decreasing grain size. Finally, the conductivity of the sample ballmilled for 48 h is enhanced by more than three decades in comparison with the coarse grained source material. All samples show Arrhenius behaviour and the activation energy is only slightly reduced in the nanocrystalline samples (0.71 eV... 0.77 eV) with respect to the microcrystalline material (0.80 eV). Therefore the enhancement of the conductivity is caused by an enhanced concentration N of mobile ions (cf. Equation 1) and/or by an enhancement of the pre-exponential factor D_0 (cf. Equation 3).

Fig. 7 displays the ^{7}Li NMR line width of microcrystalline, nanocrystalline and amorphous $LiNbO_3$ in the temperature range from 130 to 1000 K [12, 16, 17]. At low temperatures all samples show a broad line with a width of about 8 kHz (full width at half maximum) which is due to the different spin environments of the Li ions causing different local magnetic fields at the sites of the Li nuclei and thus different resonance frequencies. When the temperature is increased the ions start moving and the average local magnetic field they are sensing on the time scale of the inverse Larmor frequency becomes equal for all ions which results in the so-called *motional narrowing* of the line [3]. It sets in for microcrystalline $LiNbO_3$ at about 800 K. For the nanocrystalline and the amorphous material the narrowing starts at much lower temperatures (at about 300 K) indicating much faster Li diffusion in

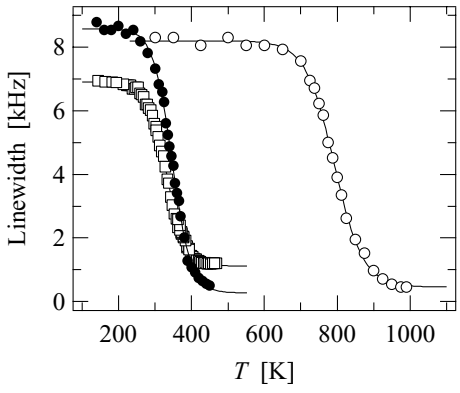

Figure 7 Motional narrowing of the ^{7}Li NMR line in microcrystalline (○), nanocrystalline (●) and amorphous (□) $LiNbO_3$ obtained at 78 MHz. The lines represent fits yielding activation energies [12].

these samples. The temperature dependence of the line width yields activation energies which are similar for the nanocrystalline and the amorphous sample (about 0.4 eV) and larger for the microcrystalline sample by a factor of about three (1.2 eV) [12]. This indicates that the diffusion pathways of the Li ions in the grain boundaries of nanocrystalline $LiNbO_3$ have amorphous-like structure. This result also corresponds to the findings for ballmilled $LiBO_2$ (cf. Section 3).

An enhancement of the diffusivity is also found for nanocrystalline BaF_2 which is an anion (F^-) conductor, see Fig. 8. The ^{19}F spin-lattice relaxation rates T_1^{-1} of micro- and nanocrystalline BaF_2 are plotted versus inverse temperature. At low temperatures (<650 K for microcrystalline BaF_2 and <300 K for nanocrystalline BaF_2) both samples show a background relaxation rate which has only a weak temperature dependence. At higher temperatures the low-temperature flank of a diffusion induced $T_1^{-1}(T)$ peak is visible in each case. The maximum of $T_1^{-1}(T)$ is expected when the jump rate τ^{-1} of the F ions approaches the Larmor frequency, i. e. when $\omega_L\tau \approx 1$ [14]. The maximum of the peak is not accessible since the nanocrystalline sample is only stable for temperatures up to about 600 K. In the microcrystalline sample the maximum is expected at temperatures above 1000 K which were not covered here. After correction for the background spin-lattice rates the

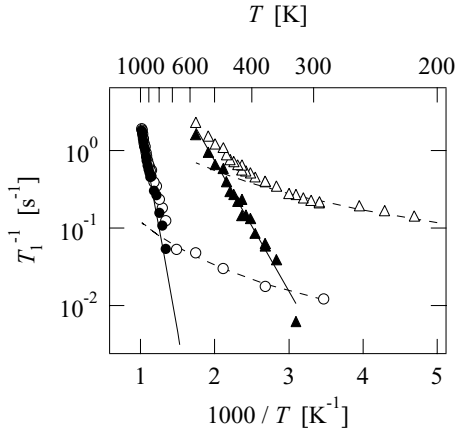

Figure 8 ^{19}F NMR spin-lattice relaxation rates T_1^{-1} for micro- (○) and nanocrystalline (△) BaF_2 vs. inverse temperature measured at 78 MHz. The full symbols represent the diffusion induced relaxation rates obtained after correction of the data for the background relaxation rate.

low-temperature flanks of the two maxima show Arrhenius behaviour and yield activation energies of 0.32 eV for nanocrystalline BaF_2 and 1.02 eV for microcrystalline BaF_2. The facts that in the nanocrystalline material the activation energy is much lower and that the diffusion induced flank is shifted to lower temperatures indicate considerably enhanced diffusivity of F ions in nanocrystalline BaF_2 and are consistent with earlier results on nanocrystalline CaF_2 [18], which, however, was not prepared by ball-milling but by inert gas condensation.

NMR spin-lattice relaxation was also studied on ^{7}Li in nanocrystalline composites of Li_2O and Al_2O_3 [19]. In contrast to monophase nanocrystalline materials, in composite systems we have, in addition to interfaces between like grains, also interfaces between unlike grains of the two different components. This gives additional possibilities to modify the network of the interfaces by variation of the composition and the grain sizes of the composites. So functional properties may be tailored by variation of these properties. The presence of interfaces between the two components can lead to surprising effects in the overall conductivity of such composites [20, 21]. The ^{7}Li magnetization transients in nanocrystalline Li_2O:Al_2O_3 composites show bi-exponential behaviour.

$$M(t) = M_{0,\,\mathrm{fast}}[1 - \exp(-t/T_{1,\mathrm{fast}})] + M_{0,\,\mathrm{slow}}[1 - \exp(-t/T_{1,\,\mathrm{slow}})] \quad (4)$$

in contrast to the microcrystalline composite where the magnetization behaviour can be described by a single exponential function

$$M(t) = M_0[1 - \exp(-t/T_1)]. \quad (5)$$

M_0 is the equilibrium magnetization in the applied magnetic field. The two relaxation rates $T_{1,\mathrm{fast}}^{-1}$ and $T_{1,\mathrm{slow}}^{-1}$ in the nanocrystalline composite can be ascribed to two different species of Li ions. This is consistent with NMR lineshape measurements on the same composites which also show two contributions [19]. Fig. 9 shows the two relaxation rates versus inverse temperature together with the relaxation rate found in the microcrystalline composites. One can see that the slower rate in the nanocrystalline composites is practically identical to that of the microcrystalline material and hence the faster Li ions can again be ascribed to the interfacial regions whose volume fraction is orders of magnitude larger in the nanocrystalline than in the microcrystalline material. It is remarkable that the activation energies of the fast and the slow Li ions in the nanocrystalline composite are equal within the experimental errors (0.30 ± 0.02 eV). This is also true for pure nanocrystalline Li_2O [22] but differs from the results on nanocrystalline $LiNbO_3$ described above. Therefore the higher diffusivity of the fast ions in the Li_2O:Al_2O_3 composites has to be explained by an enhanced preexponential factor which may indicate a higher concentration of structural defects and thus accessible sites for the Li ions in the interfacial regions.

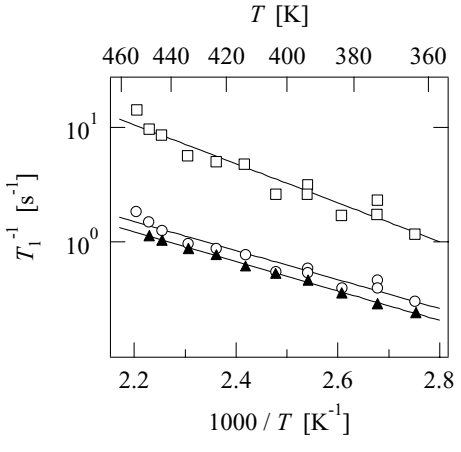

Figure 9 Discriminated ^{7}Li NMR spin-lattice relaxation rates at 58 MHz of fast (□) and slow (○) Li ions in nanocrystalline Li_2O:Al_2O_3 in comparison with the coarse grained material (▲) where only one species of Li ions is present. The lines represent fits with an Arrhenius relation.

6. Conclusion

Ball milling is suitable for preparing many different nanocrystalline ceramic materials. Highly agglomerated powders are produced which allow the investigation of interfacial diffusion. Phase transformations, in particular amorphization, have to be taken into account and will influence the microstructure of the interfacial regions. As studied both by NMR and impedance spectroscopies, in general the diffusion of mobile ions is much faster in the nanocrystalline than in the corresponding microcrystalline samples. NMR measurements reveal the presence of fast and slow ions in the nanocrystalline ceramics resulting from the heterogeneous structure with ordered crystallites and highly disordered interfacial regions. In contrast to that, in the microcrystalline counterparts only the slower species of ions is present. Therefore the fast ions in the nanocrystalline samples have to be located in the interfacial regions.

Acknowledgement

We are grateful to the Deutsche Forschungsgemeinschaft for financial support. We thank Dr. Christian Kübel (FEI Company, Eindhoven) for TEM micrographs.

References

1. H. GLEITER, *Adv. Mater.* **4** (1992) 474.
2. R. W. SIEGEL, in "Encyclopedia of Applied Physics," edited by G. L. Trigg, E. H. Immergut, E. S. Vera and W. Greulich (VCH, New York, 1994) Vol. 11, p. 173.
3. P. HEITJANS and S. INDRIS, *J. Phys.: Condens. Matter* **15** (2003) R1257.
4. *Idem.*, in "Synthesis, Functional Properties and Applications of Nanostructures" (MRS symposium proceedings), edited by H. W. Hahn, D. L. Feldheim, C. P. Kubiak, R. Tannenbaum and R. W. Siegel (Materials Research Society, Pittsburgh, 2002) Vol. 676, p. Y6.6.1.
5. S. INDRIS, D. BORK and P. HEITJANS, *J. Mater. Synth. Process.* **8** (2000) 245.
6. S. INDRIS and P. HEITJANS, *Mater. Sci. Forum* **343–346** (2000) 417.
7. S. BEGIN-COLIN, T. GIROT, A. MOCELLIN and G. LE CAËR, *Nanostruct. Mater.* **12** (1999) 195.

8. T. GIROT, S. BEGIN-COLIN, X. DEVAUX, G. LE CAËR and A. MOCELLIN, *J. Mater. Synth. Process.* **8** (2000) 139.
9. M. J. POOLEY and A. V. CHADWICK, *Radiat. Eff. Defects Solids* **158** (2003) 197.
10. E. M. GUTMAN, "Mechanochemistry of Materials" (Cambridge International Science Publishing, London, 1998).
11. C. H. RÜSCHER, E. TOBSCHALL and P. HEITJANS, in "Applied Mineralogy," edited by D. Rammlmair, J. Mederer, Th. Oberthür, R. B. Heimann and H. Pentinghaus (A.A. Balkema Publishers, Rotterdam, 2000) p. 221.
12. M. WILKENING, D. BORK, S. INDRIS and P. HEITJANS, *Phys. Chem. Chem. Phys.* **4** (2002) 3246.
13. H. P. KLUG and L. E. ALEXANDER, "X-Ray Diffraction Procedures" (John Wiley & Sons, New York, 1959).
14. P. HEITJANS and A. SCHIRMER, in "Diffusion in Condensed Matter," edited by J. Kärger, P. Heitjans and R. Haberlandt (Springer, Berlin, 1998) p. 116.
15. E. TOBSCHALL, Dissertation, Universität Hannover, 1999.
16. D. BORK and P. HEITJANS, *J. Phys. Chem.* B **102** (1998) 7303.
17. *Idem.*, *ibid.* **105** (2001) 9162.
18. W. PUIN, P. HEITJANS, W. DICKENSCHEID and H. GLEITER, in "Defects in Insulating Materials," edited by O. Kanert and J. M. Spaeth (World Scientific, Singapore, 1993) p. 137.
19. M. WILKENING, S. INDRIS and P. HEITJANS, *Phys. Chem. Chem. Phys.* **5** (2003) 2225.
20. S. INDRIS, P. HEITJANS, H. E. ROMAN and A. BUNDE, *Phys. Rev. Lett.* **84** (2000) 2889.
21. *Idem.*, *Defect Diffus. Forum* **194–199** (2001) 935.
22. S. INDRIS and P. HEITJANS, *J. Non-Cryst. Solids* **307–310** (2002) 555.

Received 11 September 2003
and accepted 27 February 2004